Life Sciences 238 (2019) 116973

Contents lists available at ScienceDirect

Life Sciences

journal homepage: www.elsevier.com/locate/lifescie

4,5-Diphenyl-2-methyl picolinate induces cellular senescence by accumulating DNA damage and activating associated signaling pathways in gastric cancer

Zhicong Zhao[a,b], Dongsheng Shang[c], Lipeng Qiu[b], Chang Guo[a], Yanyan Li[a], Hanqing Liu[c], Guoyue Yuan[a,**], Zhigang Tu[b,*]

[a] Department of Endocrinology, Affiliated Hospital of Jiangsu University, Zhenjiang, Jiangsu, 212013, China
[b] Institute of Life Sciences, Jiangsu University, Zhenjiang, Jiangsu, 212013, China
[c] School of Pharmacy, Jiangsu University, Zhenjiang, Jiangsu, 212013, China

ARTICLE INFO

Keywords:
N-heterocyclic compound
Cellular senescence
DNA damage
Gastric cancer

ABSTRACT

Aims: Gastric cancer (GC) is a common cancer with a relatively low survival rate. Cellular senescence, a potent anti-cancer mechanism, is naturally occurred, and can be induced by chemotherapeutic agents. We sought to explore new compounds against GC cells by inducing cellular senescence.

Main methods: Primary screening of a library of N-heterocyclic compounds identified some with potent inhibitory effects on GC cells. Furthermore, in vitro effects of the most potent candidate compound on the proliferation and senescence of GC cells were studied by classical assays, including senescence-associated (SA)-β-galactosidase staining, and immunofluorescence; and *in vivo* effects of this compound was evaluated in a xenograft tumor mouse model.

Key findings: Among 43 tested compounds, 4,5-diphenyl-2-methyl picolinate (DMP) showed the highest inhibition effects on the growth of GC cells. In vitro experiments showed that DMP inhibited the proliferation by inducing senescence and DNA-damage associated protein markers and signaling pathways. *In vivo* experiment confirmed that DMP treatment inhibited tumor growth by promoting DNA-damage signaling.

Significance: This study set up a platform to identify senescence-inducing anti-cancer compounds, and uncovers that DMP exerted anticancer effects by inducing cellular senescence through targeting DNA damage and associated signaling pathways in GC cancer.

1. Introduction

Gastric cancer (GC) is the fifth most prevalent type of malignancy worldwide, and is the third leading cause of cancer-related deaths [1]. China has the highest incidence of gastric cancer in the world. Three approaches, including surgery, chemotherapy, and radiotherapy, are typically used for GC treatment [2]. However, these approaches are less than optimal because of their insufficient efficacy, high relapse rate, and potential toxicities [2]. The 5-year overall survival rate of GC patients remains less than 30% [3]. To improve the overall survival rate and life quality of GC patients, new strategies against GC are urgently needed.

Recent studies have shown that cancer is associated with improper regulation of cell cycle and apoptosis [4–6]. As a state of permanent cell cycle arrest, cellular senescence has been considered as a potent anti-cancer mechanism, and can be triggered by a variety of stimuli, such as oncogene expression, oxidative stress, DNA damage, chemotherapeutics and ionizing irradiation [7–9]. Except for significant morphological alterations, senescent cells exhibit increased senescene-associated β-galactosidase (SA-β-gal), and form senescence-associated heterochromatic foci (SAHFs) which enriched in methylated H3K9, heterochromatic protein 1 (HP1), and macroH2A [10,11]. Besides, two interconnected pathways, p53/p21 and p16/RB pathways, are often activated in senescent cells [12].

Growing evidence has demonstrated that chemotherapy or radiation can inhibit tumor growth by inducing senescence and activating senescence-associated signaling pathways [13–15]. For example, dasatinib, a tyrosine kinase inhibitor, can induce senescence in non-small

* Corresponding author. Institute of Life Sciences, Jiangsu University, 301 Xuefu Road, Jingkou District, Zhenjiang, Jiangsu, 212013, China.
** Corresponding author. Department of Endocrinology, Affiliated Hospital of Jiangsu University, 438 Jiefang Road, Zhenjiang, Jiangsu, 212013, China.
E-mail addresses: yuanguoyue@ujs.edu.cn (G. Yuan), zhigangtu@ujs.edu.cn (Z. Tu).

https://doi.org/10.1016/j.lfs.2019.116973
Received 31 July 2019; Received in revised form 13 October 2019; Accepted 14 October 2019
Available online 19 October 2019
0024-3205/

cell lung cancer (NSCLC) cell that possessing kinase-inactivating BRAF mutations [16]. MLN4924, a small molecule neddylation inhibitor, was reported to inhibit the proliferation of GC cells by triggering cellular senescence *via* accumulating two cell cycle inhibitors p27 and p21 [17].

N-heterocyclic compounds are important molecules with potential anticancer activities [18–20]. In the current study, we screened a pool of 43 N-heterocyclic compounds, and identified 4,5-diphenyl-2-methyl picolinate (DMP) as the most potent compound against gastric cancer. Furthermore, we studied the possible mechanisms by which DMP exerts its anti-cancer effects, and found that DMP attenuated GC cell growth by inducing cell cycle arrest, which is accompanied with increased cell senescence by accumulating DNA damage and activating associated signaling pathways. Finally, we showed that DMP treatment significantly reduced tumor growth of GC without obvious toxicity in a xenograft tumor model.

2. Materials and methods

2.1. Chemical candidates

Compounds used in this study were mainly imidazoles, pyridines, quinolines, heterocyclic compounds and hydrazones. The chemical structures of these compounds were shown in Fig. S1.

2.2. Cell culture

Human gastric cancer cell lines, including AGS, BGC823, MKN-28 and MKN-45, and human normal gastric epithelial cell line GES-1, were obtained from American Type Culture Collection (ATCC, Manassas, VA, USA). Cancer and normal cell lines were cultured in RPMI-1640 (Gibco, Gaithersburg, MD, USA) and Dulbecco's modified Eagle's medium (DMEM, Gibco, Gaithersburg, MD, USA), respectively, with 10% fetal bovine serum (FBS, Life Technologies, Grand Island, NY, USA), 100 U/mL penicillin and 100 μg/mL streptomycin (Life Technologies, Grand Island, NY, USA), and incubated at 37 °C in an atmosphere of 5% CO_2.

2.3. MTT assay

Cell viability was assessed by MTT (3-(4,5-dimethylthiazol-2-yl)-2,5-diphenyltetrazoliumbromide, Sigma-Aldrich, St. Louis, MO, USA) assay. Cells were seeded in 96-well culture plates at 3×10^3 cells per well for 24 h. Then, different doses of candidate compounds were added into these wells for 48 h. Subsequently, 10 μL of MTT solution (10 mg/mL) was added into each well, and cells were incubated at 37 °C for additional 4 h. Next, the supernatant in each well was replaced by dimethyl sulfoxide (DMSO), and the absorbance was measured using microplate reader (Bio-Rad, Hercules, CA) at 550 nm. All the experiments were independently performed at least three times. Cell viability curves were plotted using the absorbance at each time point.

2.4. Cell apoptosis and cell cycle assays

For apoptosis assay, cells after DMP or vehicle treatment (10^6 cells per well/6-well plate) were harvested, and then double stained with Annexin V-FITC and propidium idodide (PI) using Annexin V-FITC apoptosis detection kits (Yeasen Biotechnology, Shanghai, China) according to the manufacturer's instructions. Cisplatin (Sigma-Aldrich, St. Louis, MO, USA) was used as a positive control. For cell cycle assay, DMP-treated cells (10^6 cells per well/6-well plate) were harvested, and then fixed with cold 70% ethanol at 4 °C overnight. Before flow cytometric analysis, cells were washed with cold PBS, treated with RNase A, and then stained with PI using the DNA content Quantitation kit following the manufacturer's protocol. Next, labeled cells were detected on flow cytometer (BD FACS Calibur, BD Biosciences, USA), and corresponding data were analyzed using Cell Quest software.

Table 1
IC_{50} values of 5 candidate compounds in four gastric cancer cell lines.

Candidate compounds	IC50 (μM)			
	AGS	BGC823	MKN-28	MKN-45
X-6	> 100	> 100	> 100	> 100
X-7	> 150	> 150	61.25 ± 4.12	> 150
X-14	89.52 ± 3.65	50.62 ± 1.63	38.46 ± 4.71	43.84 ± 2.84
Y-18	> 100	> 100	> 100	> 100
Y-19	45.25 ± 1.26	49.31 ± 2.24	26.52 ± 0.98	21.03 ± 3.01

2.5. Western blot analysis

DMP-treated cells (10^6 cells per well/6-well plate) were collected and lysed with ice-cold RIPA lysis buffer for 10 min, and then centrifuged at 10000 g for 1 min at 4 °C. To extract nuclear proteins, DMP-treated cells were first lysed with ice-cold buffer A [10 mM HEPES-KOH (pH = 8.0), 10 mM KCl, 1.5 mM $MgCl_2$, 0.34 M Sucrose, 10% Glycerol (pH = 7.5), 0.1% Triton X-100] for 5 min, and centrifuged at 1300 g for 5 min at 4 °C. The supernatant was removed, and the nuclei pellet was washed once with PBS, and then lysed with ice-cold RIPA lysis buffer as mentioned above. Protein concentration of the clear supernatant was quantified using a BCA protein assay kit (Beyotime Biotech., Shanghai, China). 30 μg of protein samples were used for SDS-PAGE electrophoresis. After that, the gel was transferred to a polyvinylidene difluoride (PVDF) membrane, and blocked with 5% skim milk in TBST. Next, the membrane was incubated with the relevant primary antibodies followed by HRP-conjugated secondary antibodies (Table S1). Blots were visualized with ECL plus Chemiluminescence kit (Thermo Fisher Scientific Inc., Rockford, IL, USA).

2.6. BrdU incorporation assay

DMP-treated cells (2×10^4 cells per well/24-well plate) were first incubated with 20 μM of BrdU for an hour at 37 °C, and then fixed with 4% paraformaldehyde for 10 min at room temperature. Fixed cells were permeated with 0.5% Triton X-100, treated with 0.01U/μL of DNase I and terminated with 20 mM of EDTA. Subsequently, cells were incubated with anti-BrdU-FITC in 1% of BSA for 30 min at room temperature, followed by staining with 1 μg/μL of 4′,6-diamidine-2′-phenylindole dihydrochloride (DAPI, Sigma-Aldrich, St. Louis, MO, USA), and then observed under Nikon Eclipse fluorescence microscopy. BrdU positive cells in five different high-power fields from each well were counted, and presented as mean positive cells per square micrometer. Each experiment was independently performed at least three times.

2.7. Senescence-associated (SA)-β-galactosidase staining

X-Gal (5-bromo-4-chloro-3-indolyl-β-D-galactopyranoside), a chromogenic substrate of β-galactosidase, was purchased from Sigma-Aldrich (St. Louis, MO, USA). DMP-treated cells (2×10^4 cells per well/24-well plate) were washed with PBS, and then fixed with 0.2% glutaraldehyde and 5% formaldehyde for 5 min at room temperature. Subsequently, fixed cells were washed three times with PBS, and incubated with fresh SA-β-galactosidase staining solution [1 mg/mL X-Gal, 5 mM potassium ferricyanide, 5 mM potassium ferrocyanide, 40 mM Na_2HPO_4, 150 mM NaCl, and 2 mM $MgCl_2$] at 37 °C for 4–24 h. SA-β-galactosidase positive cells were observed and counted by light microscopy, and presented as mean positive cells per square micrometer. Each experiment was independently performed at least three times.

2.8. Immunofluorescence assay

DMP-treated cells (2×10^4 cells per well/24-well plate) were

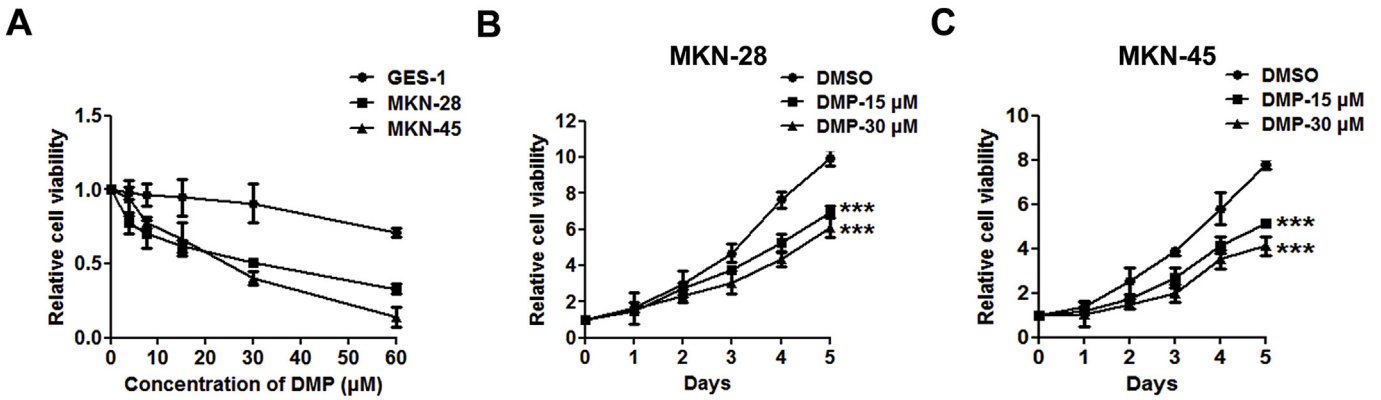

Fig. 1. The suppressive effects of DMP on proliferation of gastric cancer cells. (A) Gastric cancer cell lines MKN-28 and MKN-45, as well as normal gastric cell line GES-1 were exposed to 0–60 μM of DMP for 48 h, and their cell viabilities evaluated by MTT assay were shown in **(A)** ($n \geq 3$). MKN-28 and MKN-45 cells were treated with vehicle, 15 or 30 μM of DMP for 0–5 days, and their cell viabilities evaluated by MTT assay were shown in **(B)** and **(C)**, respectively ($n \geq 3$). $^{***}p < 0.001$.

washed with PBS, and then fixed with 4% formaldehyde for 30 min. After washing with PBS, fixed cells were permeated with 0.5% Triton X-100 for 5 min, and blocked with 3% of BSA for 30 min at room temperature. Subsequently, cells were incubated with primary antibodies anti-H3K9me3 or anti-53BP1 in 3% BSA for 2 h, followed by incubating with second antibodies for an hour in the dark, and then stained with 1 μg/μL of DAPI, and then observed under Nikon Eclipse fluorescence microscopy. Fluorescent positive cells (with > 5 foci per cell) in five different high-power fields from each well were quantified, and presented as percentage of cells positive for H3K9me3 or 53BP1 foci. Each experiment was independently performed at least three times.

2.9. In vivo tumor growth assay

All investigations were approved by the Bioethics Committee of Jiangsu University School of Medicine. Eight-week-old nude BALB/c mice were obtained from Yangzhou university medical conversion center (Yangzhou, China), bred and maintained in a pathogen-free facility. DMP was dissolved in DRD solution (10% DMSO, 5% glucose, 20% castor seed oil) before injection. For xenograft mouse model, 2×10^6 of MKN-45 cells were injected subcutaneously into the abdomen of mice. On the 14th day, tumor-bearing mice were randomly divided into four groups with six to eight mice per group, and then administrated with vehicle, 10 or 30 mg/kg of DMP, or 5 mg/kg cisplatin for every three days *via* the tail vein, respectively. Three days after six administrations, mice were sacrificed, and the tumor xenografts and main organs were removed and weighted. After that, tumor tissues were collected for further proposed studies.

2.10. Immunohistochemistry (IHC) analysis

Paraffin sections of tumor tissues were first dewaxed, rehydrated followed by antigen retrieval. Slices were then blocked with 5% BSA for an hour at room temperature, subsequently by incubation with primary antibodies against cyclin A, p53, and p21 overnight at 4 °C. After that, sample sections were incubated with corresponding horseradish peroxidase-conjugated secondary antibodies for an hour at room temperature, followed by visualization with 3,3-diaminobenzidine (DAB), and then counterstained with hematoxylin. The expression levels of proteins cyclin A, p53, and p21 were observed in situ using a bright field microscope, and then analyzed by counting nucleus positive cells in five different high-power fields. Each experiment was independently performed at least three times. The information of primary and secondary antibodies was listed in Table S1.

2.11. Statistical analysis

Data are presented as mean ± SD, unless otherwise stated. Significance was analyzed by one-way ANOVA using GraphPad Prism version 5.00 (GraphPad, San Diego, CA, USA), unless otherwise specified. $\#p > 0.05$; $^{*}p < 0.05$; $^{**}p < 0.01$; $^{***}p < 0.001$.

3. Results

3.1. DMP displayed inhibitory effects on the viability of gastric cancer cell lines

43 N-heterocyclecompounds were involved in this study, the structures of which were shown in Fig.S1. The effects of these compounds were evaluated in four gastric cancer cell lines, including AGS, BGC823, MKN-28, and MKN-45. The results showed that at the concentration of 300 μM for 48 h, ten among 43 candidate compounds exhibited significant inhibitory effects on the cancer cell growth, achieving > 80% inhibition (Fig. S2A-S2D). To identify compounds with low toxicities to normal gastric epithelial cells, the inhibitory effects of these ten compounds were further tested in human normal gastric epithelial cell line GES-1 at the same conditions. As shown in Fig. S2E, five among the ten compounds, including X-6, X-7, X-14, Y-18, and Y-19, showed no significant inhibitory effects on GES-1, indicating their relatively low toxicities. Next, different doses of the five compounds were used to treat the four gastric cancer cell lines to compare their inhibitory effects on gastric cancer cells (Fig. S3 and Table 1). The results suggested that the anti-tumor effects of the five candidate compounds on gastric cancer cells were in dose-dependent manners to some extent (Fig. S3). Among these compounds, Y-19 (4, 5-diphenyl-2-methyl picolinate, DMP) had the strongest inhibitory effect on cancer cell growth, and was selected for subsequent studies (Fig. S3 and Table 1).

3.2. DMP inhibited gastric cancer cell growth by inducing cell cycle arrest

To further clarify the inhibitory effect of DMP on cell growth, different doses of DMP were used to treat gastric cell lines MKN-28 and MKN-45, and cell viabilities were evaluated after 48 h. Compared with DMP-treated normal human gastric epithelial cell line GES-1, the viabilities of DMP-treated MKN-28 and MKN-45 cells were remarkably decreased in a dose-dependent manner, with IC50 of 26.52 μM and 21.03 μM, respectively (Fig. 1A and Table 1). Furthermore, treatment of 15 μM or 30 μM DMP for longer time also greatly reduced the viabilities of MKN-28 and MKN-45 cells (Fig. 1B and C). To explore the underlying mechanisms of the inhibitory effect of DMP on cancer cell growth, apoptosis rate, cell cycle distribution, and DNA synthesis status in DMP-

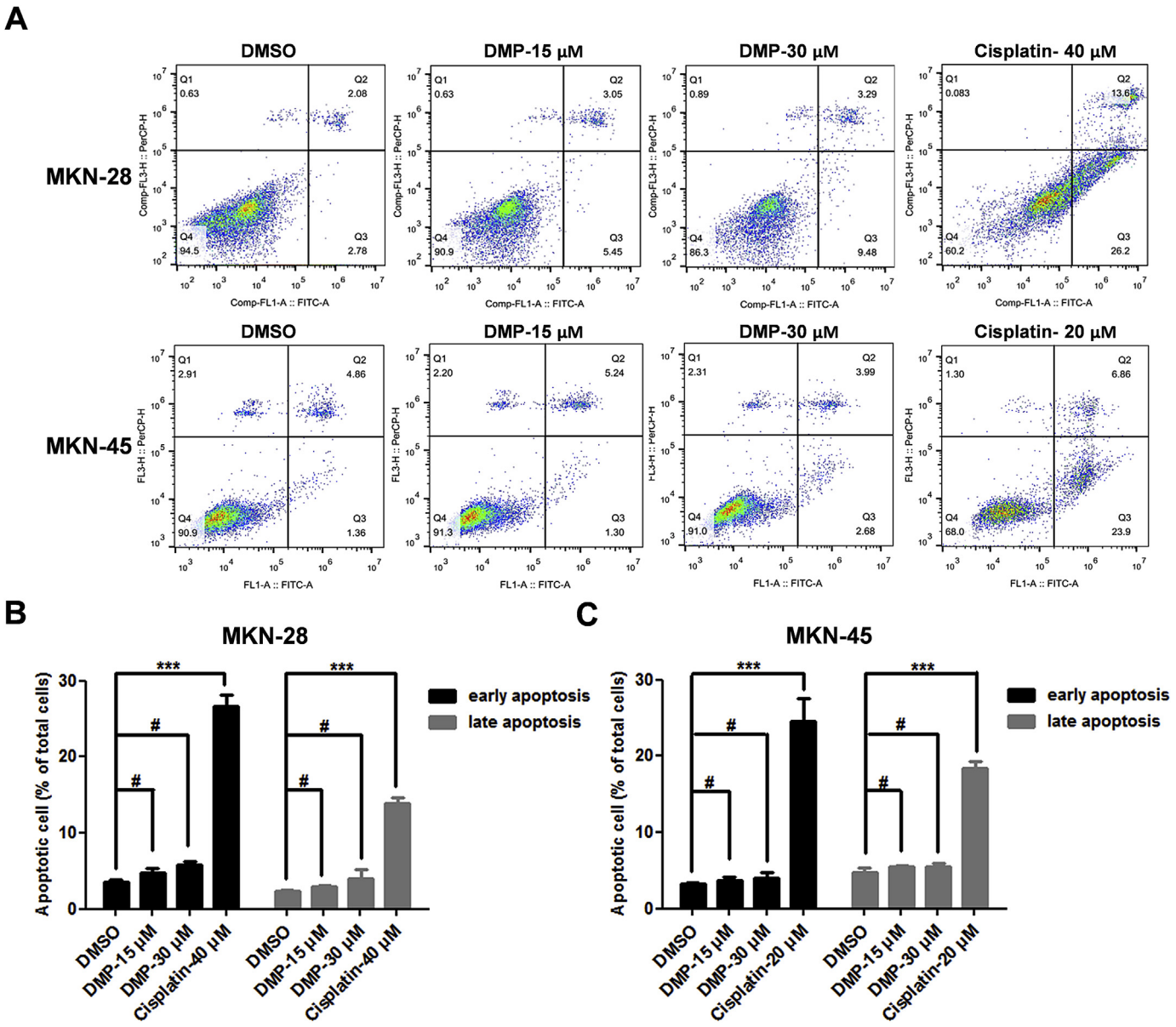

Fig. 2. DMP did not affect apoptosis of gastric cancer cells. Gastric cancer cell lines MKN-28 and MKN-45 were exposed to vehicle, 15 or 30 μM of DMP for 48 h, and apoptosis were analyzed by flow cytometry. Representative images of cells treated with DMP were shown in **(A)**, and statistical analysis graph of apoptotic MKN-28 cells and MKN-45 cells induced by DMP were presented in **(B)** and **(C)**, respectively. FL1: Annexin V-FITC; FL3: Propidium iodide (PI). The results of **A** were analyzed for the presence of Annexin V (+)/PI (−) (early apoptosis) and Annexin V (+)/PI (+) (late apoptosis). Cisplatin was used as a positive control. The results were presented as mean ± SEM from three independent experiments compared with control group. #$p > 0.05$, ***$p < 0.001$.

treated gastric cancer cells were evaluated (Fig. 2 and 3). Results from flow cytometry showed that 15 μM or 30 μM of DMP did not impact on the apoptosis of gastric cancer cells (Fig. 2A–2C); however, the same concentrations of DMP significantly increased the portion of G2/M cells and reduced the portion of G0/G1 cells, indicating that DMP could induce cell cycle arrest in G2/M phase (Fig. 3A–3C). Western blot results demonstrated that the expression of cyclin A was greatly reduced, while two other cyclins, including cyclin D1 and cyclin B, were not changed in DMP-treated gastric cancer cells **(**Fig. 3D**)**. BrdU incorporation assay suggested that DMP dramatically inhibited DNA synthesis of gastric cancer cells (Fig. 3E-3F). These data demonstrated that DMP played an inhibitory role in gastric cancer cells *via* promoting cell cycle arrest.

3.3. DMP induced senescence phenotypes in gastric cancer cells

Since senescence is correlated with permanent cell cycle arrest, we postulated that the function of DMP in cell cycle progression may associate with senescence. SA-β-gal activities and the formation of SAHF, two cellular markers of senescence, were detected in DMP-treated gastric cancer cells. As shown in Fig. 4A–4D, DMP treatment resulted in significantly enhanced number of SA-β-gal positive cells and SAHF positive cells when compared with untreated ones. H3K9me3 protein, a core element of SAHF, was accumulated in nuclear and co-localized with SAHF (Fig. 4C-4D). Western blot results suggested that expression levels of H3K9me3, as well as another SAHF protein marker HP1γ, were dramatically increased after DMP treatment (Fig. 4E–4G). Together, these data indicated that DMP induced senescent phenotypes in gastric cancer cells.

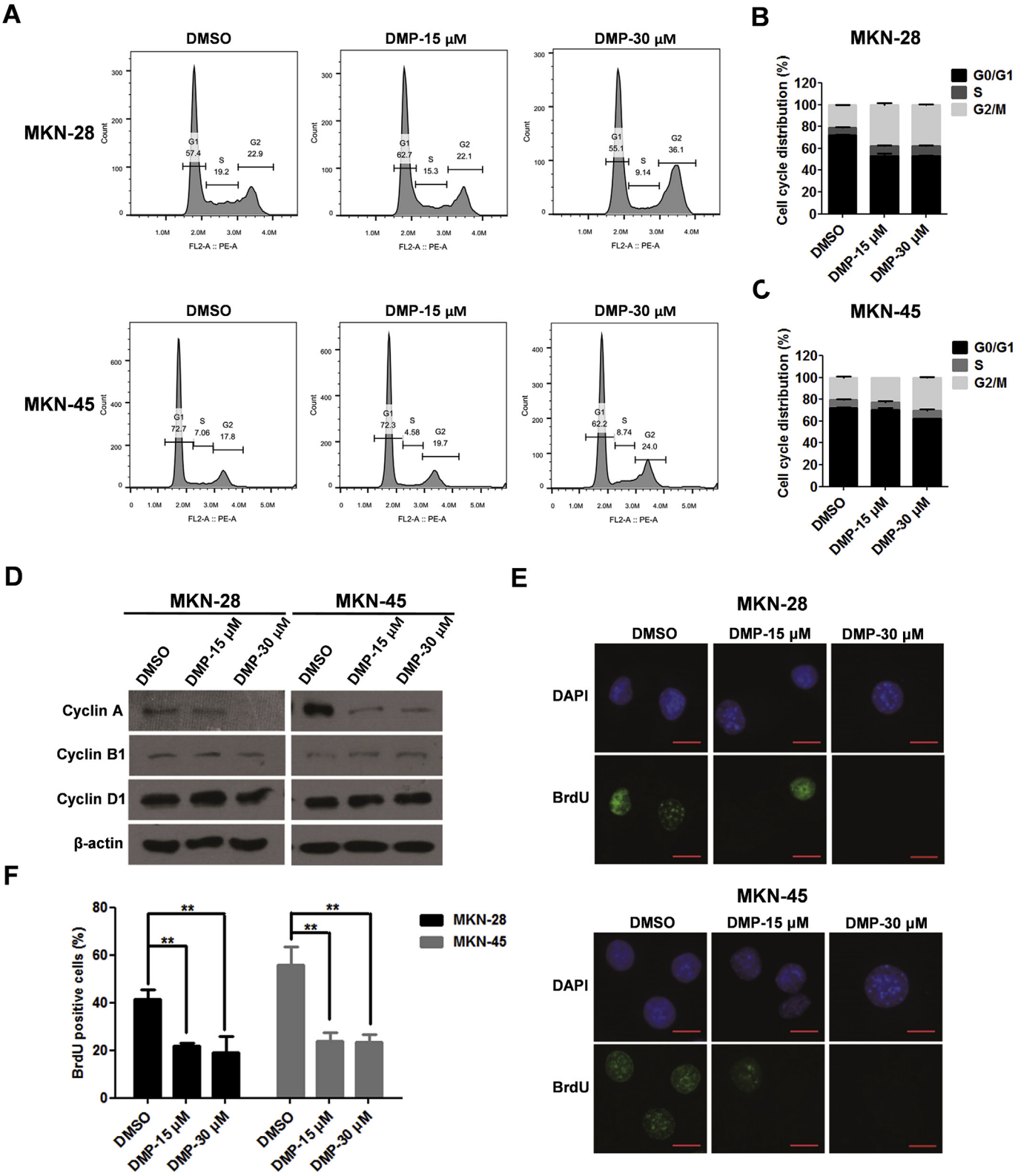

Fig. 3. DMP promoted cell cycle arrest of gastric cancer cells. Gastric cancer cell lines MKN-28 and MKN-45 were exposed to vehicle, 15 or 30 μM of DMP for 48 h, and the cell cycle progression and expression levels of cell cycle associated proteins, as well as DNA synthesis of these cells were analyzed by flow cytometry, Western blot, and BrdU incorporation assay, respectively. Representative images of cell cycle distribution by flow cytometry were shown in **(A)**, and statistical analysis graphs of cell cycle distribution of MKN-28 cells andMKN-45 cells treated with DMP were presented in **(B)** and **(C)**, respectively. Expression levels of cell cycle-associated proteins, including cyclin A, cyclin B, and cyclin D detected by Western blot were shown in **(D)**. β-actin was used as a loading control. Representative images of DNA synthesis by BrdU incorporation assay were shown in **(E)**, and statistical analysis graph of **E** was presented in **(F)**. The results were presented as mean ± SEM from three independent experiments compared with control group. $^{**}p < 0.01$.

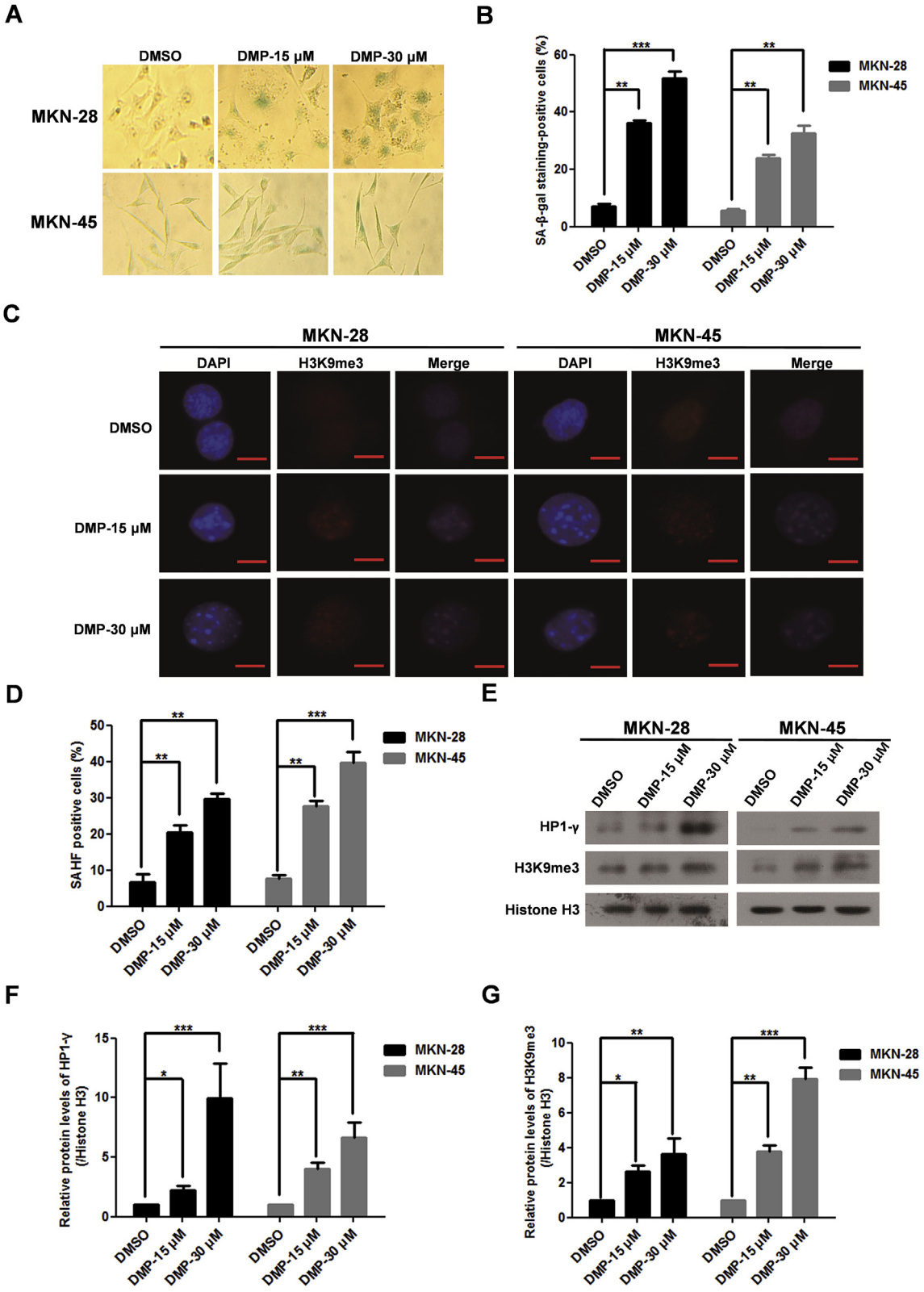

Fig. 4. DMP induced cell senescence phenotypes in gastric cancer cells. Gastric cancer cell lines MKN-28 and MKN-45 were exposed to vehicle, 15 or 30 μM of DMP for 48 h, and SA-β-gal activities and the formation of SAHF were detected using SA-β-gal staining, immunofluorescence and Western blot. Representative images of MKN-28 and MKN-45 cells treated with DMP by SA-β-gal stainining were shown in **(A)**, and statistical analysis graph of SA-β-gal positive MKN-28 and MKN-45 cells treated with DMP was presented in **(B)**. Representative images of expression levels of SAHF marker H3K9me3 by immunofluorescence was shown in **(C)**, and statistical analysis graph of SAHF positive cells treated with DMP was presented in **(D)**. H3K9me3 foci positive cells (with > 5 foci per cell) were quantified in five different high-power fields from each well, and presented as percentage of cells positive for H3K9me3 foci. Representative images of expression levels of H3K9me3 and another SAHF protein marker HP1-γ by Western blot analysis were shown in **(E)**, and statistical analysis graphs of protein expression changes of HP1-γ and H3K9me3 were presented in **(F)** and **(G)**, respectively. β-actin was used as a loading control. The results were presented as mean ± SEM from three independent experiments compared with control group. $^{*}p < 0.05$,$^{**}p < 0.01$, $^{***}p < 0.001$.

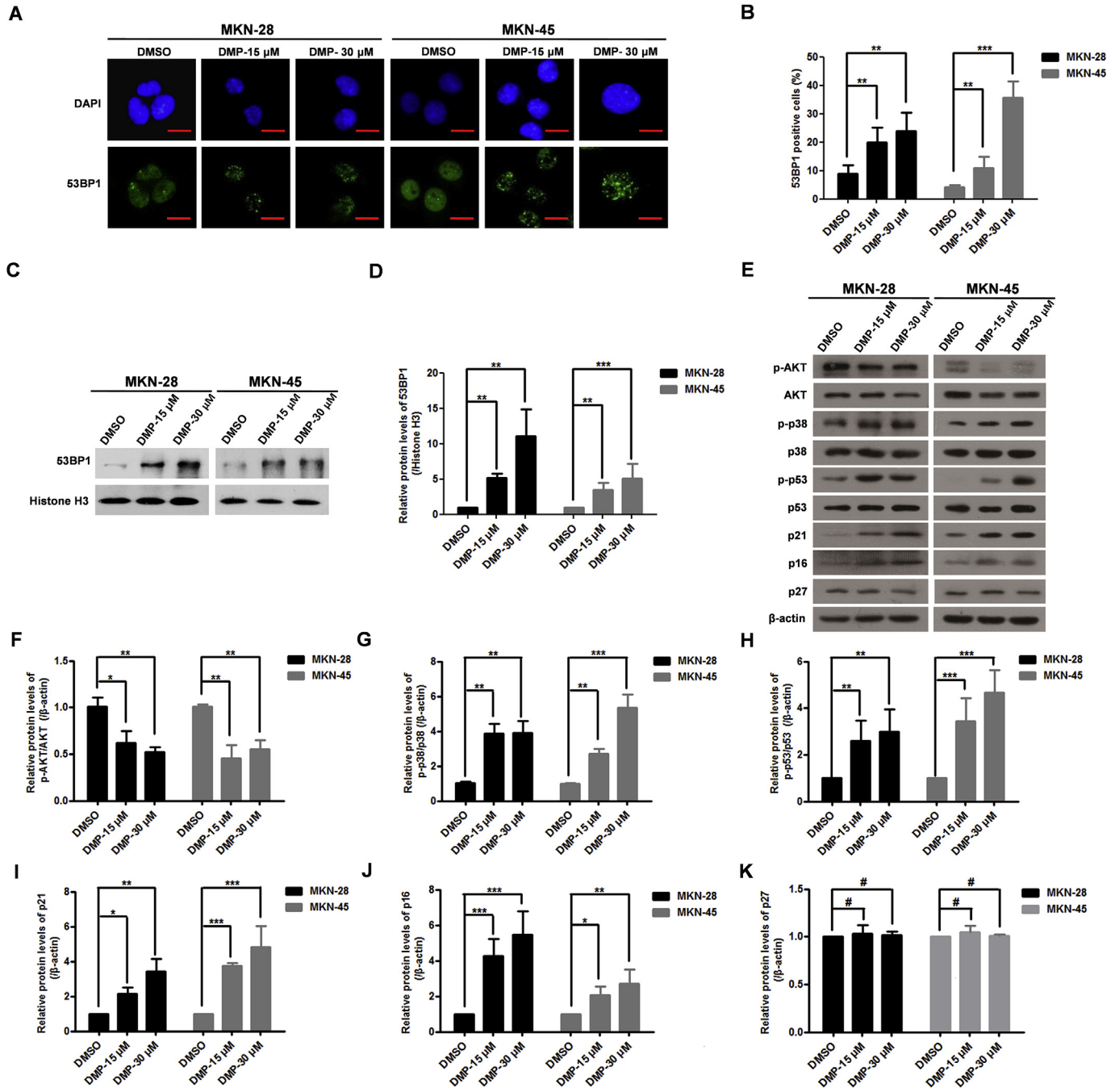

Fig. 5. DMP accumulated DNA damage and activated DNA damage-associated signaling pathways. Gastric cancer cell lines MKN-28 and MKN-45 were exposed to vehicle, 15 or 30 μM of DMP for 48 h, and the expression levels of DNA damage marker 53BP1, as well as key proteins in DNA damage-associated p53/p21 and p16/Rb signaling pathways were detected by immunofluorescence and Western blot. Representative images of expression levels of 53BP1 by immunofluorescence were shown in **(A)**, and statistical analysis graph of 53BP1 positive cells treated with DMP was presented in **(B)**. 53BP1 foci positive cells (with > 5 foci per cell) were quantified in five different high-power fields from each well, and presented as percentage of cells positive for 53BP1 foci. Representative images of expression levels of 53BP1 in nucleus by Western blots were shown in **(C),** and statistic graph of expression levels of 53BP1 in DMP-treated gastric cancer cells was presented in **(D).** Histone H3 was used as a nuclear loading control. Expression levels of key proteins in p53/p21 and p16 signaling pathways by Western blot analysis were shown in **(E),** and statistic graphs of expression changes of these proteins were presented in: pAKT/AKT **(F)**, p-p38/p38 **(G)**, p-p53/p53 **(H)**, p21 **(I)**, and p16 **(J)**. β-actin was used as a loading control. The results were presented as mean ± SEM from three independent experiments compared with control group. $^{*}p < 0.05$, $^{**}p < 0.01$, $^{***}p < 0.001$.

3.4. DMP promoted senescence by accumulating DNA damage and activating the associated signaling pathways

Growing evidence demonstrated that in response to various stressors, cell senescence often accompanied by DNA damage. To find out whether DMP induced senescence was associated with DNA damage, the expression levels of DNA damage-marker proteins, such as 53BP1, as well as key proteins in corresponding signaling pathways, such as p53/p21 and p16 signaling pathways, were detected by Western blot and immunofluorescence. Results showed that expression levels of 53BP1 was significantly enhanced in nucleus, and 53BP1 foci was greatly increased in DMP-treated cells, suggesting significant DNA

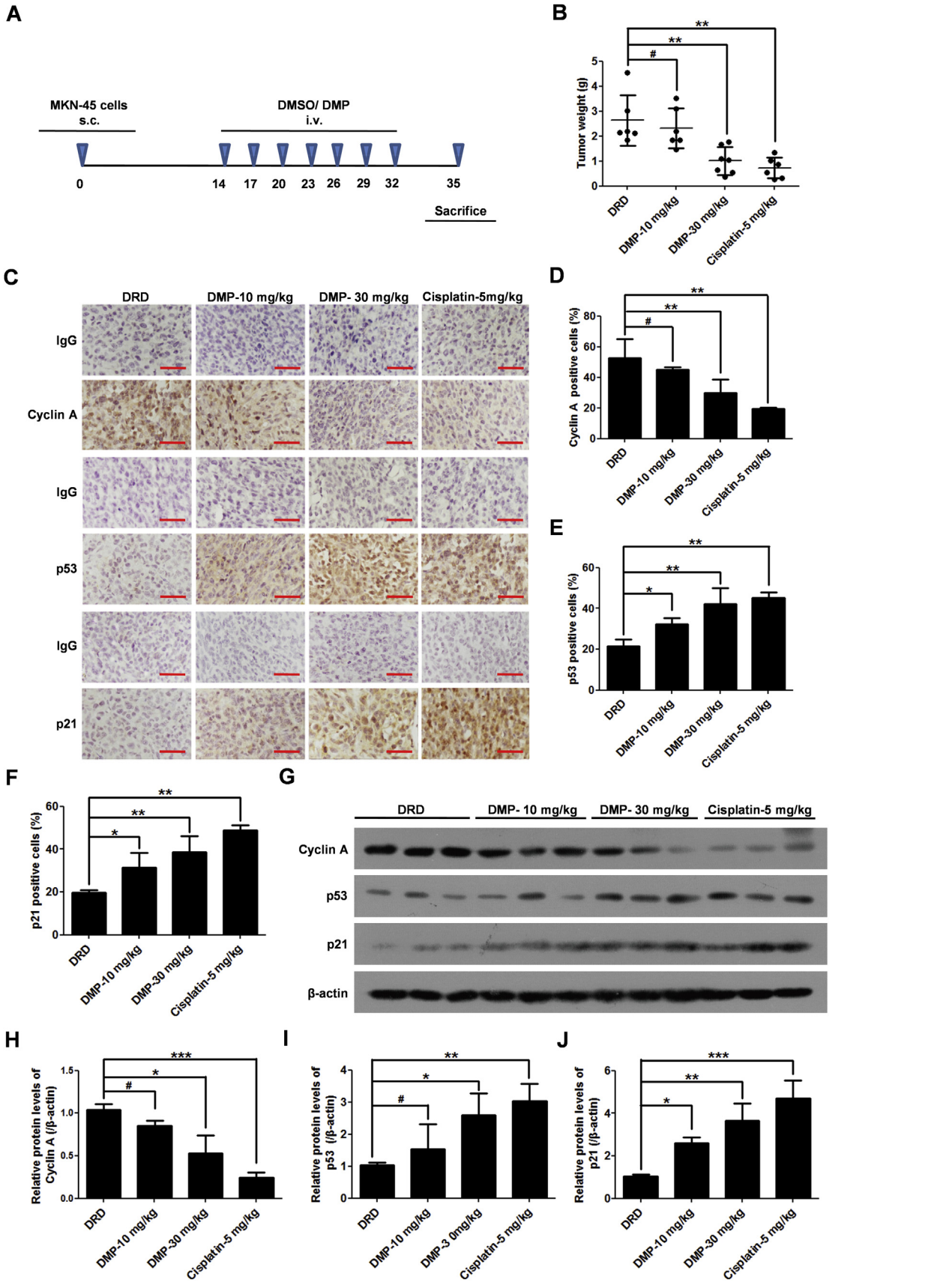

(caption on next page)

Fig. 6. DMP significantly inhibited tumor growth *in vivo*. Experimental model of subcutaneous tumor-bearing mice was shown in **(A)**. DMP was dissolved in DRD solution (10% DMSO, 5% glucose, 20% castor seed oil) before injection. MKN-45 cells were injected subcutaneously into the abdomen of mice. From 14th to 32nd day, these mice were administrated with vehicle, 10 or 30 mg/kg of DMP for every three days, and then sacrificed on the 35th day. Cisplatin was used as a positive control. *In vivo* subcutaneous tumor weights for MKN-45 cells treated with DMP were shown in (B). Representative images of expression levels of Cyclin A, p53, and p21 by immunohistometry staining were shown in **(C),** and statistic graphs of expression changes of these proteins in nucleus were presented in: Cyclin A **(D)**, p53 **(E)**, and p21 **(F)**. IgG was used as a negative control. Original magnification × 400. Representative images of expression levels of Cyclin A, p53, and p21 by Western blot were shown in **(G),** and statistic graphs of expression changes of these proteins were presented in: Cyclin A **(H)**, p53 **(I)**, and p21 **(J)**. β-actin was used as a loading control. Data were presented as mean ± SEM from three independent experiments compared with control group ($n = 8$ mice/group). $\#p > 0.05$, $*p < 0.05$, $**p < 0.01$, $***p < 0.001$.

damage in cells by DMP (Fig. 5A–5D). Furthermore, some key proteins in p53/p21 and p16/Rb signaling pathways were greatly changed in DMP-treated gastric cancer cells. Compared with vehicle-treated cells, expression levels of p-AKT were dramatically reduced; expression levels of p-p38, p-p53, p21, and p16 were greatly increased; while expression levels of p27 remained unchanged, indicating that DMP induced gastric cancer cell senescence by activating p53/p21 and p16 signaling pathways (Fig. 5E–5K).

3.5. DMP exerted significant anti-tumor activity in vivo

To evaluate the anti-tumor activity of DMP *in vivo*, a xenograft tumor model using nude mice transplanted with MKN-45 cells were established. These tumor-bearing mice were administrated with vehicle, cisplatin (5 mg/kg), or DMP (10 or 30 mg/kg) for every three days, and then sacrificed after 21 days (Fig. 6A). Tumor growth and weight loss of these mice were evaluated. The results demonstrated that compared with vehicle control, 10 mg/kg of DMP inhibited tumor growth to some extent, while 30 mg/kg of DMP showed significant inhibitory effects, leading to 66.2% reduction on tumor growth (Fig. 6B). Furthermore, 10 or 30 mg/kg of DMP did not affect body weights and organ weights of mice, also did not result in obvious pathological changes in multiple organs, suggesting relatively low toxicities of DMP on mice (Fig. S4**)**. Immunohistochemistry results indicated expression levels of Cyclin A were greatly reduced, while expression levels of p53 and p21 were dramatically increased (Fig. 6C–6F) in tumors from mice treated with DMP. Similar results were shown in western blot assay (Fig. 6G–6J). Taken together, these data demonstrated that 30 mg/kg of DMP effectively inhibited tumor growth by inducing cellular senescence in a xenograft tumor model, and may serve as a promising candidate compound for the treatment of GC.

4. Discussion

Despite great progress has been made in the treatment of cancer, GC remains to be a significant public health problem due to its high incidence and low survival rate. Thus, it is important to develop novel agents for the treatment of GC patients. In view of previous evidences that N-heterocyclic compounds demonstrated favorable anti-cancer activities, we studied a pool of 43 N-heterocyclic compounds, and found that DMP was highly effective and selective in blocking GC cell growth by inducing cell cycle arrest and cellular senescence.

As promising anticancer strategy, cellular senescence plays an important role in permanently arresting the proliferation of damaged and defective cells. Compared with possible side effects caused by higher doses of small molecule compounds, relatively lower doses of these compounds are considered safe and effective by inhibiting cancer cell growth *via* inducing cellular senescence through targeting senescence signaling regulators, such as p53, cyclin-dependent kinases (CDK), and protein kinase C (PKC), or through modulating different biological processes, including DNA damage, microtubule polymerization, DNA epigenetic modifications, as well as senescence-associated secretory phenotype (SASP) [21–23]. For example, doxorubicin, a DNA intercalator, induces cellular senescence in different cancer cells by accumulating DNA damage *via* inhibiting DNA topoisomerase II and introducing DNA double strand breaks; while paclitaxel and peloruside A, two microtubule-stabilizing agents, effectively induce senescence phenotypes of cancer cells by promoting the polymerization of microtubule and interrupting mitosis [24–27]. In the current study, we demonstrated that DMP induced cellular senescence by accumulating DNA damage and activating DNA damage-associated p53/p21 and p16 signaling pathways. This mechanism of action is of great importance considering the pivotal roles of p53/p21/p16 as tumor suppressors in DNA damage and different types of cancer. Currently, the detailed mechanism of how DMP induces DNA damage and DNA damage response signaling pathways is under investigation.

5. Conclusion

The present study indicated that DMP inhibited GC cell proliferation and revealed anticancer effects by inducing cellular senescence through targeting DNA damage and associated p53/p21 and p16 signaling pathways, rendering DMP a potential therapeutic agent for the treatment of GC. Further structure modification of this compound may generate anti-cancer agents with improved efficiency and specificity.

Declaration of competing interest

The authors have declared no conflict of interest.

Acknowledgements

This work was supported by the National Natural Science Foundation of China [Grant number 31471294, 31771521, 81672582, 1870548, 81570721, 81870548]; Natural Science Foundation of Jiangsu Province for Distinguished Young Scholars [Grant number BK20160013]; Natural Science Foundation of Jiangsu Province [Grant number BE2016718]; Top Talent of Innovative Research Team of Jiangsu Province; Six Talent Peak Project from Government of Jiangsu Province [Grant number 2015-SWYY-019, 2016-SWYY-011]; Start-up Scientific Research Fund for the Returned Oversea Scholars from Chinese Ministry of Education; Senior Talent Start-up Funds of Jiangsu University [Grant number 14JDG050, 14JDG011].

Appendix A. Supplementary data

Supplementary data to this article can be found online at https://doi.org/10.1016/j.lfs.2019.116973.

References

[1] F. Bray, J. Ferlay, I. Soerjomataram, R.L. Siegel, L.A. Torre, A. Jemal, Global cancer statistics 2018: GLOBOCAN estimates of incidence and mortality worldwide for 36 cancers in 185 countries, Ca - Cancer J. Clin. 68 (2018) 394–424.
[2] T. Waddell, M. Verheij, W. Allum, D. Cunningham, A. Cervantes, D. Arnold, Gastric cancer: ESMO-ESSO-ESTRO clinical practice guidelines for diagnosis, treatment and follow-up, Eur. J. Surg. Oncol. 40 (2014) 584–591.
[3] C. Allemani, et al., Global surveillance of cancer survival 1995-2009: analysis of individual data for 25,676,887 patients from 279 population-based registries in 67 countries (CONCORD-2), Lancet 385 (2015) 977–1010.
[4] G.I. Evan, K.H. Vousden, Proliferation, cell cycle and apoptosis in cancer, Nature 411 (2001) 342–348.
[5] K. Vermeulen, D.R. Van Bockstaele, Z.N. Berneman, The cell cycle: a review of

regulation, deregulation and therapeutic targets in cancer, Cell Prolif 36 (2003) 131–149.
[6] H.S. Kim, S. Kacew, B.M. Lee, Genetic and epigenetic cancer chemoprevention on molecular targets during multistage carcinogenesis, Arch. Toxicol. 90 (2016) 2389–2404.
[7] N. Ohtani, D.J. Mann, E. Hara, Cellular senescence: its role in tumor suppression and aging, Cancer Sci. 100 (2009) 792–797.
[8] B.D. Chang, et al., Role of p53 and p21waf1/cip1 in senescence-like terminal proliferation arrest induced in human tumor cells by chemotherapeutic drugs, Oncogene 18 (1999) 4808–4818.
[9] R. Sager, Senescence as a mode of tumor suppression, Environ. Health Perspect. 93 (1991) 59–62.
[10] D.J. Kurz, S. Decary, Y. Hong, J.D. Erusalimsky, Senescence-associated (beta)-galactosidase reflects an increase in lysosomal mass during replicative ageing of human endothelial cells, J. Cell Sci. 113 (2000) 3613–3622.
[11] R. Salama, M. Sadaie, M. Hoare, M. Narita, Cellular senescence and its effector programs, Genes Dev. 28 (2014) 99–114.
[12] S. Lee, J.S. Lee, Cellular senescence: a promising strategy for cancer therapy, BMB. Rep 52 (2018) 35–41.
[13] N.K. Han, et al., Secretome analysis of ionizing radiation-induced senescent cancer cells reveals that secreted RKIP plays a critical role in neighboring cell migration, Proteomics 12 (2012) 2822–2832.
[14] J.A. Ewald, J.A. Desotelle, G. Wilding, D.F. Jarrard, Therapy-induced senescence in cancer, J. Natl. Cancer Inst. 102 (2010) 1536–1546.
[15] H. Gali-Muhtasib, R. Hmadi, M. Kareh, R. Tohme, N. Darwiche, Cell death mechanisms of plant-derived anticancer drugs: beyond apoptosis, Apoptosis 20 (2015) 1531–1562.
[16] S. Peng, et al., Dasatinib induces DNA damage and activates DNA repair pathways leading to senescence in non-small cell lung cancer cell lines with kinase-inactivating BRAF mutations, Oncotarget 7 (2016) 565–579.
[17] H. Lan, Z. Tang, H. Jin, Y. Sun, Neddylation inhibitor MLN4924 suppresses growth and migration of human gastric cancer cells, Sci. Rep. 6 (2016) 24218.
[18] J. Akhtar, A.A. Khan, Z. Ali, R. Haider, M. Shahar Yar, Structure-activity relationship (SAR) study and design strategies of nitrogen-containing heterocyclic moieties for their anticancer activities, Eur. J. Med. Chem. 125 (2017) 143–189.
[19] Li Wen-Tai, et al., Synthesis and biological evaluation of N-heterocyclic indolyl glyoxylamides as orally active anticancer agents, J. Med. Chem. 46 (2003) 1706–1715.
[20] H. Lage, E. Aki-Sener, I. Yalcin, High antineoplastic activity of new heterocyclic compounds in cancer cells with resistance against classical DNA topoisomerase II-targeting drugs, Int. J. Cancer 119 (2006) 213–220.
[21] M. Lee, J.S. Lee, Exploiting tumor cell senescence in anticancer therapy, BMB. Rep 47 (2014) 51–59.
[22] P. Liu, et al., Cellular senescence-inducing small molecules for cancer treatment, Curr. Drug Targets 19 (2019) 109–119.
[23] N.V. Petrova, A.K. Velichko, S.V. Razin, O.L. Kantidze, Small molecule compounds that induce cellular senescence, Aging Cell 15 (2016) 999–1017.
[24] M.A. Sliwinska, et al., Induction of senescence with doxorubicin leads to increased genomic instability of HCT116 cells, Mech. Ageing Dev. 130 (2009) 24–32.
[25] E. Piegari, et al., Doxorubicin induces senescence and impairs function of human cardiac progenitor cells, Basic Res. Cardiol. 108 (2013) 334.
[26] P. Altieri, et al., Testosterone antagonizes doxorubicin-induced senescence of cardiomyocytes, J. Am. Heart. Assoc 5 (2016) e002383.
[27] A. Chan, et al., Induction of accelerated senescence by the microtubule-stabilizing agent peloruside A, Invest. New. Drugs. 35 (2017) 706–717.